Research in Astronomy and Astrophysics, 25:085013 (7pp), 2025 August

https://doi.org/10.1088/1674-4527/ade384
CSTR: 32081.14.RAA.ade384

Revealing a Major Merger in the Nearby Galaxy Group IC 1262 with Chandra Observations

Chengjing Wang[1], Yu Wang[1], Jie Xia[1], Xuliang Fan[1], and Hai-Guang Xu[2]
[1] School of Mathematics, Physics and Statistics, Shanghai University of Engineering Science, Shanghai 201620, China; wangyu@sues.edu.cn
[2] School of Physics and Astronomy, Shanghai Jiao Tong University, Shanghai 200240, China
Received 2025 February 6; revised 2025 May 24; accepted 2025 June 3; published 2025 July 1

Abstract

We analyze the deep Chandra data of the nearby IC 1262 group, and find that the bow-shaped structure, located about 17 kpc (25″) east of the X-ray peak, is a cold front moving eastward with a Mach number of $M = 0.7 \pm 0.1$. Furthermore, the line-of-sight velocity distribution of the member galaxies is clearly divided into two subgroups. Assuming the same mass-to-light ratio, the group is undergoing a major merger. Since the cooler core of the group as a whole is not destroyed by the merger, and the high-velocity subgroup has a component of eastward movement, it can be naturally explained that the cold front appears on the east side of the group center.

Key words: galaxies: groups: individual (IC 1262 group) – ISM: kinematics and dynamics – X-rays: galaxies: clusters

1. Introduction

The merging process of galaxy groups and clusters stands as one of the most energetic events in the universe (Markevitch et al. 1999). Mergers have been regarded as valuable tools for studying cosmology and galaxy formation (Smith et al. 2004), because they are an important process for the growth of galaxy groups and galaxy clusters. Cold fronts, shocks, and radio halos are formed at different stages of merging, which are typical characteristics of the merging process (Begelman et al. 1984; Markevitch & Vikhlinin 2007; Feretti et al. 2012). These features often appear in X-ray and radio observations, providing valuable information about the merging process (Hu et al. 2021; Breuer et al. 2024). They are a common subject of study in clusters, with numerous examples of shock heating of the intra-cluster medium (ICM; e.g., McNamara et al. 2005; Bourdin et al. 2013; van Weeren et al. 2017; Botteon et al. 2018; Ubertosi et al. 2023).

However, the lower density of intra-group medium (IGM) and the lower velocities of the galaxy population have led to fewer studies of group-scale mergers. The effects of non-gravitational heating, such as AGN feedback and merger shocks, are expected to be more significant in lower mass systems as the energy input from these sources is comparable to the binding energy of the group (e.g., Ponman et al. 1996; Ponman et al. 1999; Helsdon & Ponman 2000). Thus, the heating effects can affect the cooling and feedback cycle, and have a considerable impact on their constituent galaxies. Only a handful of group-group mergers with high enough velocities (e.g., Kraft et al. 2006, 2011; Randall et al. 2009; Machacek et al. 2010, 2011; Russell et al. 2014; O'Sullivan et al. 2019; Schellenberger et al. 2017; Wang et al. 2019; Rajpurohit et al. 2024) are known.

This paper presents a major merger discovered in deep Chandra observations of the nearby IC 1262 galaxy group ($z = 0.0326$; Smith et al. 2004), which is dominated by the cD galaxy IC 1262 ($17^h33^m02\overset{s}{.}0468$,$+43^d45^m34\overset{s}{.}887$, E, $M_V = -22.04$; $z = 0.03265$). The X-ray imaging analyses reveal that two surface brightness edges are evident to the east and northwest in the center of this group (Trinchieri et al. 2007; Pandge et al. 2019). The AGN activity in the IC 1262 galaxy has led to the formation of a pair of radio lobes extending roughly northward and southward, covering a distance of over 200 kpc (5′), and forming two X-ray cavities with scales of several kpc (Pandge et al. 2019), respectively. After a detailed comparison, we find that the flux centers of both the northern and southern radio lobes are located more than 22 kpc (33″) west of the optical center of the IC 1262 galaxy, and the radio lobes are two 'tails' of the galaxy. Those indicate that the cD galaxy is moving to the east.

In Section 2, we describe the Chandra observations and data reductions. In Section 3, we present the X-ray image, temperature and metal abundance distributions, and confirm a cold front. In Section 4, we analyze the velocity distribution of the identified member galaxies. In Section 5, we discuss and summarize our results. Throughout the paper, we adopt the cosmological parameters $H_0 = 73\ \mathrm{km\ s^{-1}\ Mpc^{-1}}$, $\Omega_b = 0.044$, $\Omega_M = 0.27$. Unless stated otherwise, the quoted errors stand for 90% confidence limits.

2. Observations and Data Reductions

The Chandra X-ray Observations pointing on the IC 1262 galaxy group are 2001 August 23 (ObsID 2018), 2006 April 17 (ObsID 6949), 2006 April 19th (ObsID 7321), and 2006 April

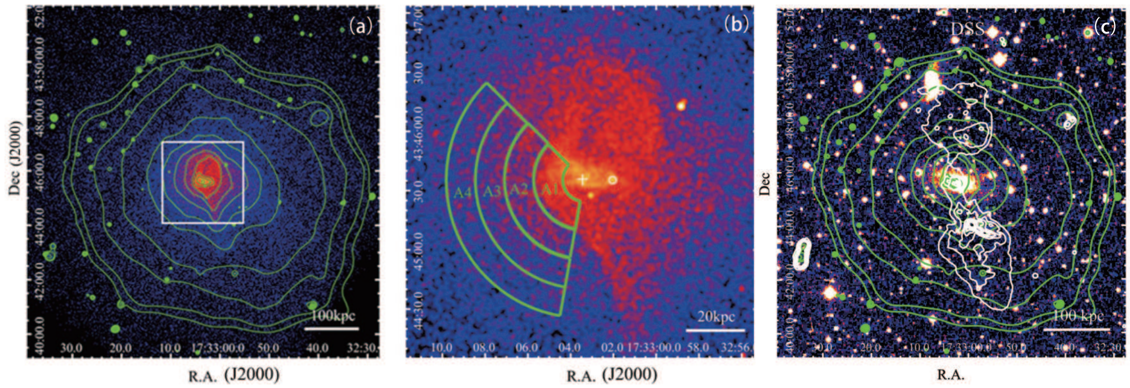

Figure 1. (a) The exposure-corrected and adaptively smoothed X-ray image of IC 1262 group in the central 521.0 kpc × 521.0 kpc (13′ × 13′) region in 0.3–2.0 keV, which has merged the observations ObsID 6949, 7321, and 7322. The X-ray contours are overlaid. (b) The X-ray image in central 120.2 kpc × 120.2 kpc (3′ × 3′) region which is a zoomed view of the white box region as shown in (a). The X-ray peak and the optical center of IC 1262 galaxy are shown as a cross and a circle, respectively. Four regions (A1, A2, A3, A4) centered are shown here to extract SBPs, and spectra in Section 3.3. (c) The DSS optical image in the same region as (a) overlaid with the X-ray contours (green) and LOFAR 143 MHz contours (white, Bírzan et al. 2020).

Table 1
Chandra Observation Log

ObsID	Observing Mode	CCDs on	Starting Date	Total Time (ks)	Clean Time (ks)
2018	VFAINT	2, 3, 5, 6, 7, 8	2001 Aug 23	32.2	30.7
6949	VFAINT	0, 1, 2, 3, 6	2006 Apr 17	38.6	38.6
7321	VFAINT	0, 1, 2, 3, 6	2006 Apr 19	37.6	37.6
7322	VFAINT	0, 1, 2, 3, 6	2006 Apr 22	37.5	37.5

22 (ObsID 7322). The data were acquired using the Advanced CCD Imaging Spectrometer (ACIS) operating in VFAINT mode. According to the standard data procedure, we processed the data using CIAO v4.14 and CALDB v4.10.2. First, we updated the level = 1 event files with the latest aspect solution files. Then, we created the new bad pixel files and reprocessed the observations using the latest calibration files provided by the Chandra X-ray Observations. We examined the 0.3–12.0 keV lightcurves extracted from the background regions defined on the ACIS-I chips, and found that there are almost no strong background flares that increased the background count rate to >115% of the mean quiescent value. The obtained net exposures are listed in Table 1.

For spectral analyses, we used Chandra spectra in the range of 0.7–7.0 keV. The background spectrum of ObsID 2018 was taken from blank sky observations, because the diffuse radiation of the IC 1262 group fills the entire CCD7. For the other three observations, the local background spectra were extracted from the outer regions of ACIS-I chips, where the background is relatively clean. The results from the blank sky background spectra and the local background spectra are consistent. During the spectral analyses, we used the SPECEXTRACT tool to create the appropriate auxiliary response files (ARF) and redistribution matrix files (RMF). The spectra were fitted with an absorbed APEC model coded in the XSPEC. The hydrogen column density $N_{\rm H}$ was fixed at the Galactic value of $1.58 \times 10^{20}\,{\rm cm}^{-2}$ (Ben Bekhti et al. 2016), and the redshift was fixed at that of the group, while the gas temperature and metal abundance were set as free parameters.

3. Results

3.1. X-ray Imaging Analyses

In Figure 1(a), we show the ACIS-I image of the IC 1262 galaxy group in the 0.3–2.0 keV, which has been corrected for exposure but not for background. The image is obtained by merging the observations ObsID 6949, 7321, and 7322. We enlarge the X-ray central region of the group, as shown in Figure 1(b). We find that the X-ray peak (R.A. = $17^{\rm h}33^{\rm m}03\overset{\rm s}{.}2978$, decl. = $+43^{\rm h}45^{\rm m}35\overset{\rm s}{.}717$) is offset from the optical center of the IC 1262 galaxy by approximately 9.1 kpc ($13\overset{''}{.}6$, $1'' = 0.668$ kpc). Additionally, we see a bow-shaped structure about 17 kpc (25″) to the east of the X-ray peak, which is extending from the center to the northeast and southeast sides, and another arc-shaped structure about 40 kpc (1′) to the northwest of the X-ray peak. Both of the structures are consistent with those reported by Trinchieri et al. (2007).

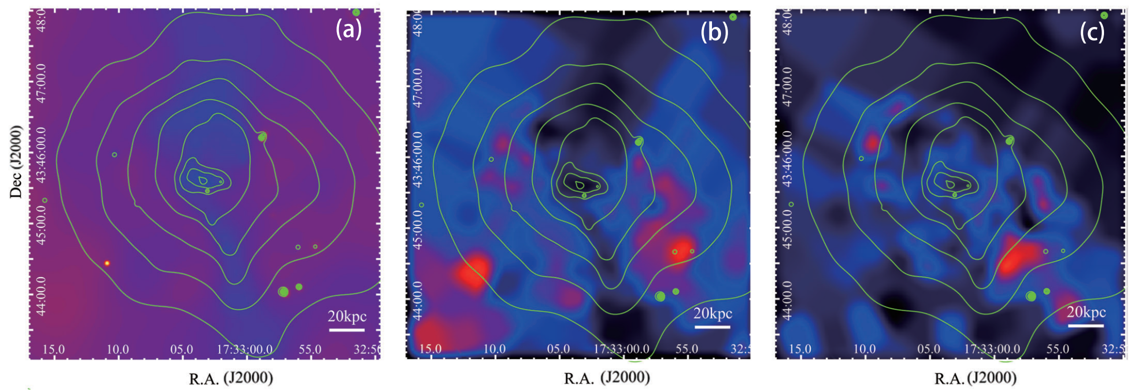

Figure 2. (a) The background-subtracted, exposure-corrected, smoothed hardness ratio map obtained through dividing the X-ray image in 2.0–5.0 keV by that in 0.3–1.2 keV in the central 200.4 kpc × 200.4 kpc (5′ × 5′) region for IC 1262 group. The gas temperature map (b) and the metal abundance map (c) in the center of the IC 1262 group. All the maps are overlaid with the X-ray contours.

In Figure 1(c), we present the optical image of the IC 1262 galaxy group overlaid with the X-ray contours and LOFAR 143 MHz contours (Bírzan et al. 2020), the latter of which show two radio lobes extending roughly toward the northwest and southwest directions, covering a distance of over 200 kpc (5′). The flux centers of two radio lobes are located more than about 22 kpc (33″) west of the optical center of IC 1262 galaxy. Those indicate that the cD galaxy is moving eastward, and leaving the radio lobes previously ejected toward north and south in their original directions as "two tails." The eastward motion of the cD galaxy is possibly the reason for the formation of the eastern bow-shaped structure.

3.2. Temperature and Metal Abundance Distributions

We show the background-subtracted, exposure-corrected, and adaptively smoothed hardness ratio map in Figure 2(a), which is created through dividing the X-ray image in the high energy band (2.0–5.0 keV) by that in the low energy band (0.3–1.2 keV). The hardness ratio inside the bow-shaped structure (∼0.36) is lower than that outside (∼0.54). On the whole, the hardness ratio is roughly lower on the north and south sides of the X-ray peak, consistent with the direction of the two radio lobes as shown in Figure 1(c), while the hardness ratio is generally higher on the east and west sides.

To obtain more accurate temperature and abundance distributions, we perform spectral analyses of IC 1262 group, using three 2006 observations (ObsID 6949, 7321 and 7322). We fit each spectrum using the absorbed APEC model. The resulting temperature and abundance maps are shown in Figures 2(b) and (c), respectively. We find that the group has a cold core with a temperature of about 1.3 keV with a radius of 10 kpc, and the temperature inside the bow-shaped structure (∼1.5 keV) is lower than the outside temperature (∼2.2 keV). On the outside, the gas temperatures on the north and south sides of the center of IC 1262 group are roughly low (1.3–1.7 keV), corresponding to the positions of the radio lobes in the radio map caused by AGN activity. Meanwhile, the temperatures on the east and west sides are high (∼2.4 keV). As shown in Figure 2(c), we find no high metallicity regions in the center, while a region with high metal abundance (∼1 $Z_\odot$) is located about 37 kpc (55″) southwest of the X-ray peak of the group.

3.3. A Cold Front

To quantitatively study the bow-shaped structure, we extracted the exposure-corrected X-ray surface brightness profile (SBPs) in 0.3–2.0 keV from the annuli restricted in an angle as shown in Figure 1(b). We present the SBPs in Figure 3(a), which exhibits a significant surface brightness discontinuity at the radius of 17.0 kpc (25.″4). These results are consistent with those of Pandge et al. (2019). Such discontinuities in surface brightness are typically caused by abrupt changes in gas density accompanied by rapid temperature variation, often indicating the presence of shocks or cold fronts (e.g., Hu et al. 2021).

We extract the spectra in the four annuli limited in the angle as shown in Figure 1(b). We show the gas temperature and metal abundance distributions in Table 2. Across the bow-shaped edge, the gas temperature in the outer region (Region A2; $2.30^{+0.16}_{-0.14}$ keV) is significantly higher than that in the inner region (Region A1; 1.69 ± 0.06 keV) at the 90% confidence level, which confirms the existence of the temperature jump. In Figure 3(b), we present the two-dimensional fit-statistic contours between temperature and metal abundance for Regions A1 and A2, corresponding to confidence levels of 68%, 90%, and 99%, respectively.

We fit the surface brightness profiles using a truncated power-law and β model (Wang et al. 2019), which is parameterized as

$$n_g(R) = \begin{cases} n_{g,1}(R/R_{\rm cut})^{-\alpha} & R < R_{\rm cut} \\ n_{g,2}[1 + (R/R_{\rm c})^2]^{-3\beta/2} & R \geqslant R_{\rm cut} \end{cases}, \quad (1)$$

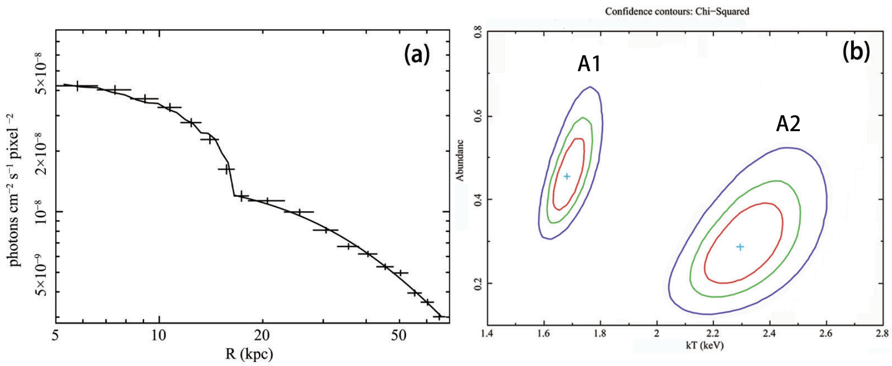

Figure 3. (a) Surface brightness profile in 0.3–2.0 keV extracted from the annuli limited in the angle shown in Figure 1(b). Solid lines show the best fits obtained with the truncated power-law and β model. (b) Fit-statistic contours at 68%, 90% and 99% confidence levels for gas temperature and metal abundance derived with the APEC model in Region A1 and Region A2.

Table 2
Gas Temperature and Metal Abundance Distributions

Region	Radius (h_{73}^{-1} kpc)	$N_{\rm H}$ (10^{20} cm^{-2})	T (keV)	Z ($Z_\odot$)	χ^2/dof
A1	7.0−17.0	fixed	1.69 ± 0.06	$0.45^{+0.11}_{-0.09}$	137.44/78
A2	17.0−27.0	fixed	$2.30^{+0.16}_{-0.14}$	$0.29^{+0.12}_{-0.09}$	139.85/78
A3	27.0−37.0	fixed	$2.25^{+0.16}_{-0.15}$	$0.32^{+0.12}_{-0.10}$	90.08/78
A4	37.0−47.0	fixed	$2.16^{+0.15}_{-0.14}$	$0.28^{+0.11}_{-0.09}$	109.01/78

Note. An absorbed APEC model is used to fit the spectra extracted from Regions A1, A2, A3 and A4, as shown in Figure 1(b). The redshift and absorption are fixed at $z = 0.0326$ and the Galactic value $N_{\rm H} = 1.58 \times 10^{20}$ cm^{-2} (Ben Bekhti et al. 2016), respectively.

where $n_{g,1}$ and $n_{g,2}$ are the electron number densities, $R_{\rm cut}$ is the truncation radius, α is the truncated power-law index, and β is the index. The best-fit values are listed in Table 3. We show the gas parameters inside and outside of the bow-shaped structure in Table 4, where the density jump is by a factor of 2.0 ± 0.2 across the bow-shaped edge.

Based on the one-dimensional fluid model and following the method of Vikhlinin et al. (2001), we simply estimate the gas pressure at the stagnation point (P_1) using the gas temperature T1 and electron number density $n_{g,1}$ measured in Region A1. We consider Region A2 as the free-flowing region and estimate its gas pressure (P_0) using the gas temperature T2 and electron number density $n_{g,2}$. Thus, we obtain the pressure ratio is $P_1/P_0 = 1.5 \pm 0.2$. Using the Bernoulli equation (Landau & Lifshitz 1959), we derive the Mach number $\mathcal{M} = 0.7 \pm 0.1$, corresponding to a velocity of 550 ± 80 km s^{-1}. Based on the above analyses, including the discontinuity in the surface brightness profile, the discontinuity in gas density and temperature distribution, as well as the Mach number and the corresponding velocity, we confirm the presence of a cold front located 17.0 kpc east of the X-ray peak of IC 1262 galaxy group, which supports that the group is undergoing a merge.

3.4. The Outer Substructures of the IC 1262 Galaxy Group

In Figure 4(a), we show the X-ray residual map of the IC 1262 group in 0.3–3.0 keV, which is obtained by subtracting an angular average β model from the exposure-corrected image. We find some diffuse emission about 390 kpc (594″) northeast of the X-ray peak, which is consistent with the location of a bright galaxy CGCG 226-028 ($17^{\rm h}33^{\rm m}20^{\rm s}.3954$,$+43^{\rm d}54^{\rm m}48^{\rm s}.604$, $M_p = -20.19$; $z = 0.03622$). We extract the surface brightness profile in this direction, as shown in Figure 4(c). We find an excess over a β model where the brightness exceeds about 6×10^{-11} photons cm^{-2} s^{-1} pixel^{-2} in the range of 364–480 kpc (545″–719″). The SBPs excess is largely associated with the location of CGCG 226-028 galaxy.

In Figure 4(b), we present the metal abundance map in the region of about 560 kpc × 560 kpc (14′ × 14′). We find a high-abundance region approximately 230 kpc (350″) north of the X-ray peak. We extract the spectra from an elliptical region, and the obtained metal abundance is $0.9^{+0.9}_{-0.4}$ $Z_\odot$ at the 68% confidence level, which is significantly higher than that of its surrounding areas (0.3 ± 0.03 $Z_\odot$). The metal abundance in other areas that appear to show a high value is consistent with that of its surrounding areas at the 68% confidence level.

4. Velocity Distribution

To investigate the merging status of the IC 1262 group, we select galaxies from the NED within a radius of 22′ centered on the weighted centroid of the galaxy distribution ($17^{\rm h}33^{\rm m}02^{\rm s}.005$,$+43^{\rm d}45^{\rm m}35^{\rm s}.0$, Laganá et al. 2013). To include possible galaxies, a velocity cut centered on the group redshift with a range of ± 2000 km s^{-1} is applied. As a result, 34 galaxies are identified as belonging to the group.

Table 3
Acceptable Fits to the Surface Brightness Profiles across the Bow-shaped Edge

	$n_{g,1}$ (10^{-3} cm^{-3})	α	$R_{\rm cut}$ (h_{73}^{-1} pixel)	$n_{g,2}$ (10^{-3} cm^{-3})	β	$R_{\rm c}$ (h_{73}^{-1} kpc)	χ^2/dof
A-region	5.64± 0.13	$0.23^{+0.06}_{-0.08}$	$51.88^{+0.08}_{-0.20}$	$3.28^{+0.03}_{-0.02}$	0.549± 0.004	117.5± 0.8	17.70/12

Note. A truncated power-law and β model is used to fit the SBPs, extracted from the annuli restricted in the angle as shown in Figure 1(b). The best-fit parameters obtained from the fitting are shown in the table.

Table 4
Gas Parameters across the Bow-shaped Edge

Region	n_g (10^{-3} cm^{-3})	T (keV)	$P = n_g T$ (10^{-3} keV cm^{-3})
A1	2.99± 0.15	1.69± 0.06	5.1± 0.3
A2	$1.50^{+0.08}_{-0.09}$	$2.30^{+0.16}_{-0.14}$	3.5± 0.3

Note. Gas temperature in Region A2 is assumed as that of the free stream from the bow-shaped edge.

First, we plot the line-of-sight velocity histogram of 34 member galaxies in the IC 1262 group in Figure 5(a). The galaxies are clearly divided into two parts: one subgroup with the higher velocity of $v > 9750$ km s^{-1}, comprising 19 galaxy members (including the cD galaxy IC 1262), and the other subgroup with the lower velocity of $v < 9750$ km s^{-1}, comprising 15 galaxy members. We perform a fit to the histogram using a single Gaussian model, and the reduced χ^2/d.o.f. is 41.9/15 (>2). Using the K-S test, we find the confidence level of the velocity distribution following a Gaussian distribution is less than 20%. Then the single Gaussian model is excluded. We use a double Gaussian model to fit it, and the reduced χ^2/d.o.f. is 5.7/12 (<0.5). The lower velocity part of the galaxy group is described by a Gaussian component with an average velocity of $\langle v_1 \rangle = 9,280^{+80}_{-170}$ km s^{-1} and a corresponding variance of $\sigma_{v,1} = 320^{+80}_{-120}$ km s^{-1}. The higher part is described with an average velocity of $\langle v_2 \rangle = 9,960^{+30}_{-20}$ km s^{-1} and a variance of $\sigma_{v,2} = 110^{+20}_{-30}$ km s^{-1}. According to the F-test, the higher Gaussian component is required at the 99% confidence level. We show the galaxies of the low-velocity subgroup as red circles, and those of the high-velocity subgroup as green circles in Figure 5(c). No significant anisotropic distribution is found on the sky plane, yet.

To further study the distribution of galaxies, we refine the line-of-sight velocity distribution of the galaxy members, with a bin size of 80 km s^{-1}, as shown in Figure 5(b). There are seven galaxies (including the cD galaxy IC 1262) in a narrow bin, and we plot these galaxies in the optical image (Figure 5(c)) as white boxes. Three of the galaxies (including IC 1262 galaxy) are very near on the sky plane, within 10 kpc (15″). The above indicates that the three galaxies, which are close in both the line-of-sight velocity and the sky plane, are dynamically integrated as a whole, and dominate the movement of the high-velocity subgroup.

The IC 1262 group is undergoing a merger between the high-velocity subgroup dominated by the cD galaxy IC 1262 and the low-velocity subgroup with IC 1263 as its main galaxy.

5. Discussion and Summary

Based on our X-ray analyses, we find that the X-ray bow-shaped structure about 17 kpc (25″) to the east of the IC 1262 galaxy group is a cold front moving eastward with the Mach number of $M = 0.7 \pm 0.1$ and the corresponding velocity of 550 ± 80 km s^{-1}. Furthermore, the line-of-sight velocity distribution of the member galaxies is clearly divided into two subgroups, which indicates that the galaxy group is undergoing a merger.

In Section 4, the brightest galaxy of the low-velocity group is IC 1263 ($M_V = -20.77 \pm 0.64$), while the cD galaxy of the high-velocity subgroup is IC 1262 ($M_V = -22.04 \pm 0.21$). According to hierarchy theory of structure formation, and assuming the same mass-to-light ratio, the mass ratio of the merger between the low-velocity subgroup and the high-velocity subgroup is roughly 1:3. When using almost all of the member galaxies (15 low-velocity galaxies and 18 high-velocity galaxies) whose near-infrared magnitudes can be found in NED,[3] the obtained mass ratio is about 2:3. Those above support that the merger is most likely to be a major merger. Here, we do not use the velocity variance ratio of two subgroups to calculate the merger mass ratio, because the number of member galaxies of each subgroup are small and the uncertainty of error will be large.

In Figure 2(b), the central region of the IC 1262 group shows a lower temperature (about 1.3 keV), which suggests the group has a cooler core. In Section 4, the cD galaxy IC 1262 and its neighboring two galaxies, all of which belong to the high-velocity subgroup, are very close in terms of both visual velocity and sky plane. So far, during the merging

[3] Noted that only several visual magnitudes of the member galaxies can be found in NED. In order to include as many member galaxies as possible, we use the absolute magnitudes in the near-infrared range.

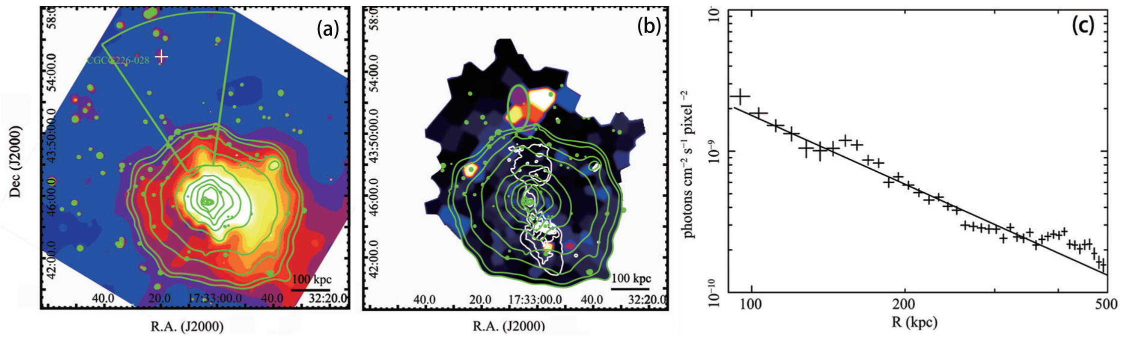

Figure 4. (a) Exposure-corrected and smoothed X-ray residual map in 0.3-3.0 keV for 785.6 kpc × 785.6 kpc (19.″6 × 19.″6) of IC 1262 group, overlaid with the X-ray contours, the cross represents the galaxy CGCG 226-028. (*b*) The metal abundance map in the same region as (a), overlaid with the X-ray contours (green) and LOFAR 143 MHz contours (white, Bírzan et al. 2020). The major axis of the ellipse where we extract the spectra is 116.0 kpc (173.″4), and the minor axis is 55.0 kpc (82.″2). (c) The radial surface brightness profile in 0.3–2.0 keV extracted from the northern annuli as shown the angle in (a). The solid lines show the best fits obtained with the β model.

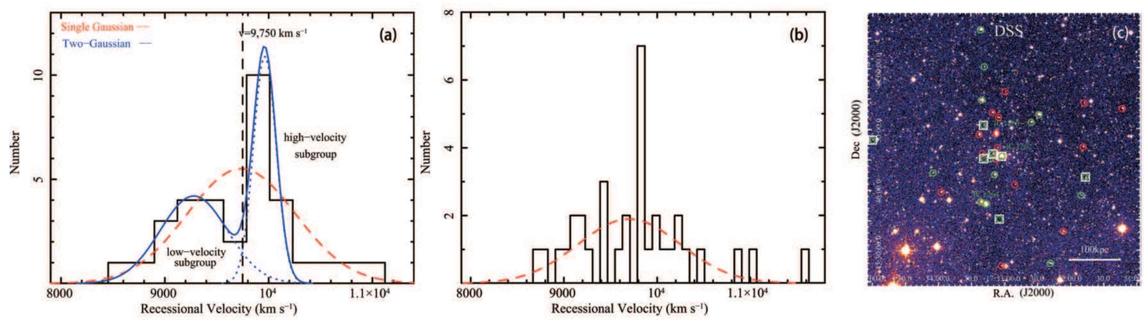

Figure 5. (a) Line-of-sight velocity distribution of 34 galaxy members identified in the IC 1262 group. The distribution is fitted with a two-Gaussian model (solid) and a single Gaussian model (dashed), respectively. (b) The refined velocity distribution in a bin of 80 km s^{-1}. The red dashed line represents the single Gaussian model. (c) The DSS optical image covers the central 1803.6 kpc × 1803.6 kpc (45′ × 45′) region of the group. The white boxes represent the galaxy IC 1262 and other galaxy members in the same velocity bin, as shown in Figure 5(b). The red circles represent the galaxy members of the low-velocity subgroup ($v < 9750$ km s^{-1}), while the green circles represent the galaxy members of the high-velocity subgroup ($v > 9750$ km s^{-1}).

process, the cooler core of the group as a whole has not been destroyed by the merger. In the radio map (Figure 1(c)), the two radio lobes caused by previous AGN activity show as two tails of galaxy IC 1262, which indicates the galaxy is moving eastward. Thus, the high-velocity subgroup dominated by the cD galaxy IC 1262 has a component of eastward movement. Therefore, it can be naturally explained that the cold front appears on the east side of the group center.

The speed of the high-velocity subgroup has a velocity of ∼680 km s^{-1} relative to the low-velocity subgroup along the line-of-sight direction. The cold front is moving eastward roughly in the plane of the sky. According to the Pythagorean Theorem, the high-velocity subgroup has a comprehensive velocity of 870 ± 190 km s^{-1} to the low-velocity subgroup. For the environment of IC 1262 group, the corresponding Mach number is >0.9. This indicates that the group is one of the strong candidates for detecting shock waves, although we have not detected them yet in the group.

In Section 3.4, we find a region with higher metal abundance about 230 kpc (350″) north of IC 1262 galaxy, which is roughly adjacent to the northern boundary of the north-side radio lobe as shown in Figure 4(b). To analyze the reason for its formation, following the method of Sarazin (1986) and Churazov et al. (2001), we calculate the cooling time as 2.9×10^{10} yr and the buoyant time as 2.5×10^{9} yr, the latter of which is one order of magnitude smaller than the former. Those cannot definitively support that the appearance of the high abundance region is caused by AGN activity of IC 1262 galaxy, because the merger of the galaxy group is an important reason for the transfer of gas abundance outside (Hu et al. 2021).

Acknowledgments

We thank the Chandra team for making data available via the High Energy Astrophysics Science Archive Research Center (HEASARC). This work was supported by the National Natural Science Foundation of China (grant Nos. 11103057 and 12003014).

References

Begelman, M. C., Blandford, R. D., & Rees, M. J. 1984, RvMP, 56, 255
Ben Bekhti, N., Flöer, L., Keller, R., et al. 2016, A&A, 594, A116
Bírzan, L., Rafferty, D. A., Brüggen, M., et al. 2020, MNRAS, 496, 2613
Botteon, A., Gastaldello, F., & Brunetti, G. 2018, MNRAS, 476, 5591
Bourdin, H., Mazzotta, P., Markevitch, M., Giacintucci, S., & Brunetti, G. 2013, ApJ, 764, 82
Breuer, J. P., Werner, N., Mernier, F., et al. 2024, arXiv:2411.08103
Churazov, E., Brüggen, M., Kaiser, C. R., Böhringer, H., & Forman, W. 2001, ApJ, 554, 261
Feretti, L., Giovannini, G., Govoni, F., & Murgia, M. 2012, A&ARv, 20, 54
Helsdon, S. F., & Ponman, T. J. 2000, MNRAS, 315, 356
Hu, D., Xu, H., Zhu, Z., et al. 2021, ApJ, 913, 8
Kraft, R. P., Forman, W. R., Jones, C., et al. 2011, ApJ, 727, 41
Kraft, R. P., Jones, C., Nulsen, P. E. J., & Hardcastle, M. J. 2006, ApJ, 640, 762
Laganá, T. F., Martinet, N., Durret, F., et al. 2013, A&A, 555, A66
Landau, L. D., & Lifshitz, E. M. 1959, Fluid Mechanics (Oxford: Pergamon Press)
Machacek, M. E., Jerius, D., Kraft, R., et al. 2011, ApJ, 743, 15
Machacek, M. E., O'Sullivan, E., Randall, S. W., Jones, C., & Forman, W. R. 2010, ApJ, 711, 1316
Markevitch, M., Sarazin, C. L., & Vikhlinin, A. 1999, ApJ, 521, 526
Markevitch, M., & Vikhlinin, A. 2007, PhR, 443, 1
McNamara, B. R., Nulsen, P. E. J., Wise, M. W., et al. 2005, Natur, 433, 45
O'Sullivan, E., Schellenberger, G., Burke, D. J., et al. 2019, MNRAS, 488, 2925
Pandge, M. B., Sonkamble, S. S., Parekh, V., et al. 2019, ApJ, 870, 62
Ponman, T. J., Bourner, P. D. J., Ebeling, H., & Böhringer, H. 1996, MNRAS, 283, 690
Ponman, T. J., Cannon, D. B., & Navarro, J. F. 1999, Natur, 397, 135
Rajpurohit, K., O'Sullivan, E., Schellenberger, G., et al. 2024, ApJ, 976, 64
Randall, S. W., Jones, C., Kraft, R., Forman, W. R., & O'Sullivan, E. 2009, ApJ, 696, 1431
Russell, H. R., Fabian, A. C., McNamara, B. R., et al. 2014, MNRAS, 444, 629
Sarazin, C. L. 1986, RvMP, 58, 1
Schellenberger, G., Vrtilek, J. M., David, L., et al. 2017, ApJ, 845, 84
Smith, R. J., Hudson, M. J., Nelan, J. E., et al. 2004, AJ, 128, 1558
Trinchieri, G., Breitschwerdt, D., Pietsch, W., Sulentic, J., & Wolter, A. 2007, A&A, 463, 153
Ubertosi, F., Gitti, M., Brighenti, F., et al. 2023, ApJ, 944, 216
van Weeren, R. J., Andrade-Santos, F., Dawson, W. A., et al. 2017, NatAs, 1, 0005
Vikhlinin, A., Markevitch, M., & Murray, S. S. 2001, ApJ, 551, 160
Wang, Y., Lui, F., Shen, Z., et al. 2019, ApJ, 870, 132